Electrophysiological receptor mapping of $GABA_A$ receptors

Alexander D Shaw[1], Hannah Chandler[1], Khalid Hamandi[1], Suresh D Muthukumaraswamy[2], Alexander Hammers[3], Krish D Singh[1].

[1]Cardiff University Brain Research Imaging Centre (CUBRIC), School of Psychology, Cardiff University, CF24 4HQ
[2]School of Pharmacy, Faculty of Medical and Health Sciences, University of Auckland, Auckland, New Zealand
[3] School of Biomedical Engineering and Imaging Sciences, King's College London, St Thomas' Hospital, London SE1 7EH

Corresponding Author: Dr Alexander D Shaw[1], shawa10@cardiff.ac.uk

Word counts:
Abstract: 342
Introduction: 819
Methods: 1257
Results: 1000
Discussion: 968

Figures: 9
Tables: 0
Supplementary Materials: **Yes**

Declarations: none.

Abstract

The non-invasive study of cortical oscillations provides a window onto neuronal processing. Temporal correlation of these oscillations between distinct anatomical regions is considered a marker of functional connectedness. As the most abundant inhibitory neurotransmitter in the mammalian brain, γ-aminobutyric acid (GABA) is thought to play a crucial role in shaping the frequency and amplitude of oscillations, which thereby suggests a further role for GABA in shaping the topography of functional connectivity. This study explored the effects of pharmacologically blocking the reuptake of GABA (increasing local concentrations and availability) through oral administration of the GAT1-blocker tiagabine (15 mg). We show that the spatial distribution of connectivity effects corresponds to template maps of flumazenil PET maps of $GABA_A$ receptor distribution.

In a placebo-controlled crossover design, we collected resting MEG recordings from 15 healthy male individuals prior to, and at 1-, 3- and 5- hours post, administration of tiagabine and placebo pill. Using amplitude envelope correlations (AECs) we quantified the functional connectivity in discrete frequency bands across the whole brain, using the 90-region Automatic Anatomical Labelling atlas (AAL90), as well as quantifying the average oscillatory activity at each region.

Analysis of variance in connectivity using a drug-by-time (2x4) design revealed interaction effects, accompanied by main effects of drug and time. Post-hoc permutation testing of each post-drug recording against the respective pre-drug baseline revealed consistent reductions of a bilateral occipital network spanning theta, alpha and beta frequencies, and across 1- 3- and 5- hour recordings following tiagabine, but not placebo.

The same analysis applied to the activity of each region also revealed a significant interaction, with post-hoc permutation testing signalling significant reductions in activity in middle occipital regions across delta, theta, alpha and beta frequency bands.

Crucially, we show that the spatial distribution of both connectivity and activity changes with tiagabine overlaps significantly with template quantitative $GABA_A$ maps derived from flumazenil volume-of-distribution (FMZ-V_T) PET, clearly demonstrating a mechanistic link between GABA availability, $GABA_A$ receptor distribution and low-frequency network oscillations. We therefore propose a utility for functional connectivity and activity measures as receptor-mapping tools in pharmacological imaging.

Introduction

Oscillations measured using non-invasive methods, such as magnetoencephalography (MEG), arise from the synchronous oscillatory-activation of post-synaptic currents in ensembles of principal cells in cortex (Brunel & Wang, 2003; Buzsáki et al., 2004; Wang, 2010), predominantly those in superficial layers (Buzsáki et al., 2012; Xing et al., 2012). Converging evidence from experimental (Kramer et al.,

2008; M. a Whittington et al., 1995) and computational (Brunel & Wang, 2003; Pinotsis et al., 2013; Shaw et al., 2017) studies suggests that the attributes of these oscillations – the peak frequency and amplitude – are determined by more fundamental, unobserved, neurophysiological processes. For example, the peak frequency of oscillations within the alpha range (8 – 13 Hz) may be a mechanistic consequence of synchronised firing (action potentials) at the same rate (Halgren et al., 2017; Lorincz et al., 2009), while the peak frequency of oscillations across many frequency bands has been linked with inhibitory neurotransmission (Buzsáki et al., 2004; Hall et al., 2011; Roopun et al., 2006; M. A. Whittington et al., 2000) mediated by γ-aminobutyric acid (GABA).

The link between GABA and macroscopic oscillations observed in MEG is likely mediated by the functional inhibitory role of GABA receptors, which are broadly categorised as fast, ionotropic $GABA_A$ and slower g-protein coupled $GABA_B$, although there exist subtypes of each (Belelli et al., 2009; Vargas, 2018; Whiting, 2003). The currents mediated by both of these receptor types have been implicated in oscillation generation through control of recurrent excitatory-inhibition (Atallah & Scanziani, 2009; Brunel & Wang, 2003; Galarreta & Hestrin, 1998; Kohl & Paulsen, 2010; Krupa et al., 2014), whereby the GABAergically-mediated inhibitory currents exert temporal control over the firing and activity of excitatory principal cells (Bartos et al., 2007; M. A. Whittington et al., 2000). In the case of higher-frequency oscillations, including beta (13 - 30 Hz) and gamma (30+ Hz), the peak frequency may be dependent on the balance of excitatory and inhibitory currents (Brunel & Wang, 2003; Kujala et al., 2015; Shaw et al., 2017), implicating excitatory glutamatergic receptor types, such as α-amino-3-hydroxy-5-methyl-4-isoxazolepropionic acid (AMPA) and N-methyl-D-aspartate (NMDA).

Pharmaco-MEG studies provide a framework for examining the effects that pharmacologically manipulating neurotransmitter or neuromodulator systems has on oscillatory activity. Studies of GABAergic drugs to date have primarily examined changes in task-induced fluctuations in oscillation metrics, usually confined to the analysis of one particular sensory system. For example in the motor cortex, diazepam, a benzodiazepine, facilitates the amplitude of movement-related beta desynchrony (MRBD) (Hall et al., 2011). In visual cortex, propofol, an agonist of $GABA_A$ receptors, increased the amplitude of gamma oscillations and concurrently suppressed the amplitude of alpha oscillations (Saxena et al., 2013). Alcohol, which has a complex binding profile including benzodiazepine-mediated $GABA_A$ effects, decreased the frequency and increased the amplitude of gamma in the visual cortex (Campbell et al., 2014). For other GABAergic pharmaco-MEG summaries, see ((Suresh D Muthukumaraswamy, 2014; Nutt et al., 2015)) These studies clearly demonstrate a role for GABA in shaping oscillatory responses, however they are confined to observations of task-related, local dynamics.

Non-task induced recordings of oscillatory activity, at ‘resting state’, focus on correlation of fluctuations in different brain regions, within specific frequency bands. This ‘functional connectivity’ approach rests on the assumption that discrete regions of the brain whose band-limited amplitude

envelopes are correlated, are functionally connected. Since GABA plays a role in shaping the oscillations of local (within-region), task-induced dynamics, it is expected that it also shapes the topography of the networks formed by these regions interacting.

No pharmaco-MEG studies have examined GABAergic manipulation of functional connectivity across the brain, although studies examining other compounds have. Antagonism of NMDA receptors by ketamine decreased alpha and beta networks spanning motor, parietal and occipital regions (S. D. Muthukumaraswamy et al., 2015), while antagonism of AMPA receptors by perampanel increased alpha and beta in similar posterior visual and parietal regions (Routley et al., 2017). Comparison of the spatial distribution of these reductions with recent maps of receptor distributions (Zilles & Palomero-Gallagher, 2017) revealed that these areas also have higher-than-average densities of NMDA and AMPA receptors in superficial cortical layers, as well as higher-than-average densities of $GABA_A$ and $GABA_B$ receptors (where the average is calculated over the 44 cortex-wide regions tested) (Zilles & Palomero-Gallagher, 2017).

In the present study, we examined the effect of pharmacologically blocking the reuptake of GABA using tiagabine, a GABA-transporter 1 (GAT1) blocker. We anticipated that, at rest, increased GABA availability would lead to increased activation of GABAergic receptors and thereby GABAergic inhibition, which would have a macroscopic effect of reducing functional connectivity strengths across frequency bands.

Having identified regions demonstrating tiagabine-induced band-limited changes in connectivity and activity, we next examined the degree to which these changes overlap with the spatial distribution of GABA-A receptors in a template of flumazenil volume-of-distribution (FMZ-V_T) PET. Here, we expected the volume-of-distribution of FMZ-V_T (interpreted as the density of GABA-A receptors), to correspond to the regions showing the biggest drug-induced changes in connectivity and activity.

Materials and Methods

MEG Methods

Sample

Fifteen healthy individuals (1 female, 14 male) aged between 20 – 32 (mean 25.5) completed a single-blind, placebo-controlled crossover study of 15mg oral tiagabine (Gabatril) and placebo. Study days were separated by at least a week, with each day consisting of 4 MEG scans; an initial ‘pre-drug’ recording, followed by post-ingestion scans at 1-, 3- and 5 hours. Data from this study, including a full overview of the design, has been published previously (Magazzini et al., 2016; Suresh D Muthukumaraswamy et al., 2013). All study participants gave informed consent and the study procedures were approved by the UK National Research Ethics Service (South East Wales). Volunteers were excluded if they reported personal history of psychiatric or neurological diagnosis,

current recreational or prescription drug use, or impaired liver function, indicated by conventional liver function test.

Data Acquisition

Whole head MEG recordings were obtained using a CTF275 radial gradiometer system, with participants seated upright. Task-free, 'resting' recordings of 10 minutes were obtained at 1200 Hz and analysed as synthetic third-order gradiometers (Vrba, 2001). Participants were fitted with three electromagnetic head coils (nasion and bilateral pre-auriculars), which remained fixed throughout the study day, and were localized relative to the MEG system immediately before and after recording. All study participants had a T1-weighted MRI (1mm isotropic) available for subsequent source-space analysis. Co-registration was achieved by placement of fiduciary markers at fixed distances from anatomical landmarks easily identifiable on an anatomical MRI (tragus, eye centre). Offline, recordings were down-sampled to 600 Hz and segmented into 2 s epochs. Segments were visually inspected for gross artifact (e.g. movement, clenching, eye blinks), which were disregarded.

Analysis Pipeline

The present analysis sought to compute the functional connectivity between a set of spatially resolved brain loci. We chose to compute this using the amplitude envelope correlation (AEC) metric, which is interpretable, robust and repeatable (Colclough et al., 2016). This coupling was computed separately for 7 distinct frequency bands using conventional band edges; delta (1 – 4 Hz), theta (4 – 8 Hz), alpha (8 – 13 Hz), beta (13 - 30 Hz) and 3 gamma windows (40 – 60, 60 – 80 and 80 – 100 Hz). Figure 1 shows a graphical representation of the analysis pipeline, which is detailed below.

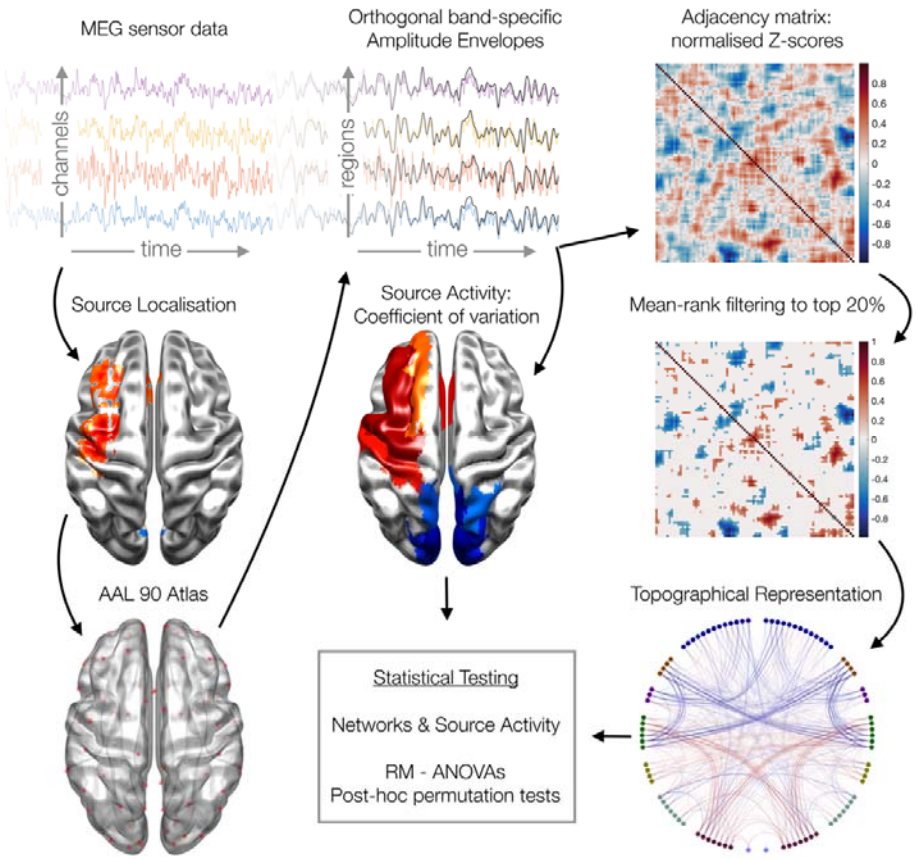

Figure 1. Schematic overview of the analysis and statistical pipeline.

Source analysis was performed using the linearly constrained minimum-variance (LCMV) beamformer, a spatial filtering method, as implemented in Fieldtrip (Oostenveld et al., 2011). We used a local-spheres conductivity (forward) model to estimate MEG sensor measurements as a function of the activity of a series of discrete sources inside the head, arranged on a 6 mm grid. Using this information, along with the covariance of the MEG channels, the beamformer estimated the temporal activity of each of the nodes in the 6 mm grid (inside the head), as linear combinations of the MEG channels. This step was repeated for each of the frequency bands of interest, with the covariance of the MEG channels being recomputed from appropriately band-pass filtered data.

We next reduced the spatial dimensionality of the source reconstructed data to a set of 90 anatomical loci, described by the Automatic Anatomical Labelling (AAL90) atlas. For each of the 90 AAL regions, we computed the temporal coefficient of variation (CoV; standard deviation / mean) of all the reconstructed grid sources falling within that AAL regions' proximity (cortical parcel). We chose one grid source to represent each AAL90 region, selected based on the largest CoV (that is, the voxel showing the largest temporal variation about its mean).

Having reduced to a set of 90 regions, the temporal activity of these sources was orthogonalized with respect to each other region using symmetric orthogonalization (Colclough et al., 2015), which further

reduces source leakage. Next, the amplitude envelopes of each region were extracted using the absolute of the (complex) analytical signal derived by Hilbert transform (in MATLAB). These amplitude envelopes were used for both the source-activity and functional connectivity analyses.

Functional Connectivity

The functional connectivity of the 90 regions was calculated using cross-correlations of the amplitude envelopes of each region. Since correlations are undirected, only the upper triangular portion (minus the diagonals) of the 90-by-90 correlation matrix was computed, requiring 3960 computations for each of the frequency bands tested, for each subject.

Inspection of the histogram of the resulting matrices revealed a bi-modal distribution comprising a null distribution, centred around 0, along with a positive tail-like distribution. In order to model this null distribution (noise), we z-scored the matrix according to the mean and standard deviation of a Gaussian fitted to the null. Finally, we thresholded the resulting matrix, retaining only the top 20% strongest connections (rank-sorted).

Source Activity Analysis

We computed estimates of the source activity in each frequency band, at each of the 90 regions, using the temporal CoV. This measure represents the amount of 'activity' (deviations around the mean) of the region while remaining relatively insensitive to global changes in, for example, baseline power. Thus, it is a measure of activity, not power.

PET Flumazenil Methods

Sample

A group of 16 healthy participants (females: 4, age range: 26-61 years, mean age: 46 years) had been recruited as healthy controls for a larger clinical PET study. No participants included in the study reported a history of neuropsychiatric or neurological conditions or were on any prescribed medications. None of the participants consumed alcohol within 48 hours prior to their PET-FMZ scan. All participants provided written informed consent according to the Declaration of Helsinki. Approvals from the UK Administration of Radioactive Substances Advisory Committee (ARSAC) and the Ethics Committee, Imperial College, Hammersmith Hospital, were obtained. For the creation of the FMZ template, data from six healthy participants with global values close to the mean were selected and raw and right-left reversed (flipped) data were used (12 scans).

PET scan parameters and image analysis

All PET data were collected on a 953B Siemens/CTI PET scanner. Dynamic 3D PET data were collected, which consisted of 20 frames over a 90-minute time period. Scans were obtained with axial planes parallel to a horizontal plane passing through the anterior and posterior commissures. The tracer, ~370 MBq of [^{11}C]FMZ, was injected intravenously and arterial blood samples were collected

in order to calculate the plasma input function with metabolite correction (Lammertsma et al., 1993) (Hammers et al., 2003).

Voxelwise parametric maps of [^{11}C]FMZ total volume-of-distribution (V_T) were calculated from the time-series data and arterial plasma input functions with spectral analysis (Cunningham & Jones, 1993; Lassen et al., 1995), allowing for a blood volume fraction, as detailed previously (Hammers et al., 2008).

Template creation

Statistical Parametric Mapping software was used to create the [^{11}C]FMZ PET template (SPM99, Wellcome Department of Cognitive Neurology, London, UK, https://www.fil.ion.ucl.ac.uk/spm/software/spm99/).

PET data were coregistered to the corresponding MRI data, and left-right-reversed, but not resliced. The MRIs were then normalised to the Montreal Neurological Institute standard space (MNI152). The PETs were spatially normalised using the same transformations as for the MRI images and written out with voxel sizes of 2 mm x 2 mm x 2 mm. Data were then averaged with a softmean function and smoothed with an 8 mm (FWHM) Gaussian kernel to yield the final template.

Statistical Analyses

For both connectivity and activity analyses, we employed a repeated-measures analysis of variance (RM-ANOVA), of drug (tiagabine, placebo) by time (pre and 1-, 3- and 5-hours post). Where main effects indicated, we employed permutation-based paired-*t* testing with omnibus-correction to facilitate post-hoc interpretation of effects. For the comparison of spatial distribution of effects with the PET FMZ template, we used randomisation-based Pearson's correlations (5000 permutations) with omnibus correction.

Results

Functional Connectivity

Figure 2 shows connections (edges) demonstrating significant drug-by-time interaction for each frequency band (top row), as well as edges showing a main effect of drug (middle row) and session (bottom row), as computed by rm-ANOVA. Connections showing significant interaction effects were observed in alpha (n=83), beta (62), theta (61) and delta (7) bands, with most connections clustered around posterior regions (occipital / parietal). There were no edges in the gamma range demonstrating an interaction effect (figure 2 demonstrates only gamma[1], 40 – 60 Hz, however the negative result was also observed in the higher gamma bands). Connections showing a main effect of drug were observed in theta (n=96), alpha (58), beta (33) and delta (20), largely confined to posterior regions but including interactions with cingulate and temporal regions in the alpha band. Effects of session were observed across all frequency bands (130 in alpha, 111 in beta, 48 in theta, 22 in delta

and 3 in gamma[1]). Again, these were posteriorly focussed but included interactions with frontal, deep (delta) and temporal (theta) regions. A list of the top-5 strongest (significant) edges for each frequency band, and each term (effect), are listed in supplementary table 1.

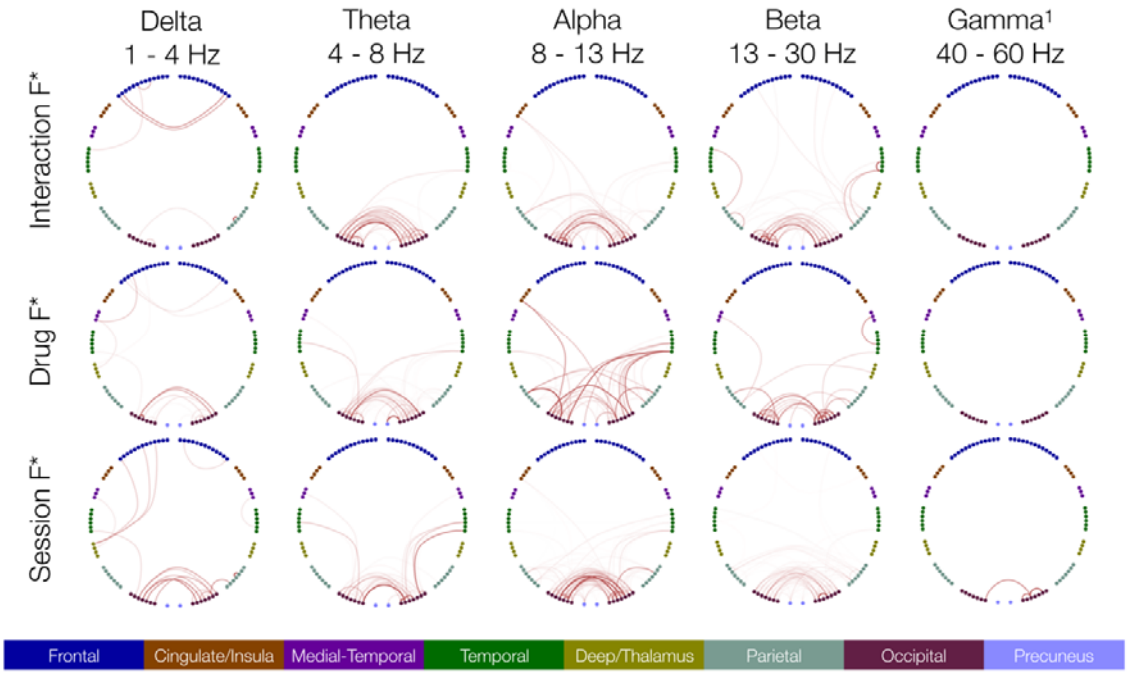

Figure 2. Topographical representation of the significant (p<.05) connections (edges) from the RM_ANOVA, showing interaction effects (top row), as well as drug (row 2) and session / time effects (row 3). Colour key at bottom describes regions, left/right represents hemisphere.

Post-hoc permutation-based randomisation testing of within-drug session effects revealed significant reductions (figure 3, blue lines) of edge strength for tiagabine at 1-, 3- and 5- hr vs. pre, across delta, theta, alpha and beta. Analysis of the topography revealed these reductions were confined to occipital cortices. Increases were observed at two frontal edges (1 at 3 hours, 1 at 5 hours) in the delta band. Significant increases in edge strength were observed between frontal and temporal regions (3 hours vs pre) and temporal and deep regions (5 hours vs pre) across all three gamma windows for placebo. No other within-drug-vs.-pre changes in edge strength were observed for placebo. A list of all significant edges for each frequency band and each comparison (n=6; 1-, 3- and 5- hours vs. pre for each drug) are listed in supplementary table 2.

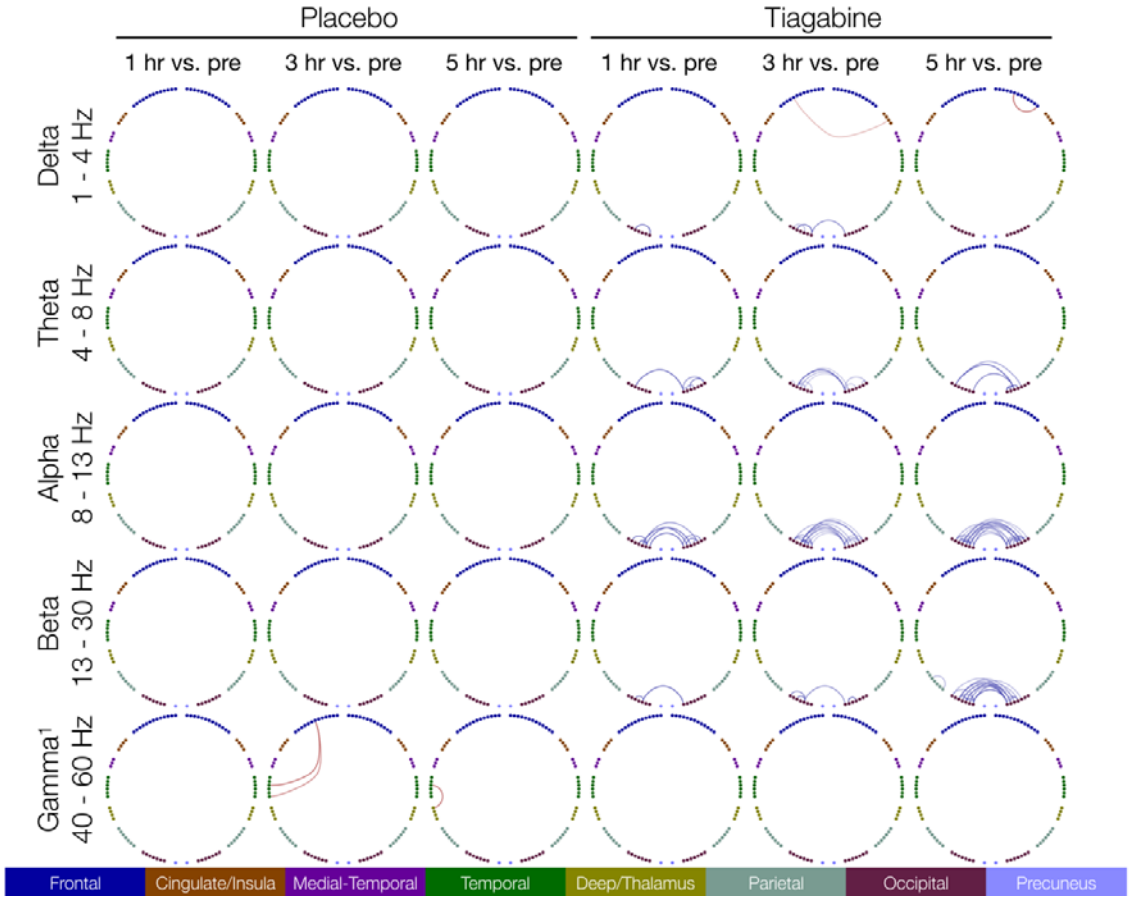

Figure 3. Topographical representation of the post-hoc permutation-based (5k) tests, showing only significant (p<.05) connections, for within-drug comparisons to baseline (1-, 3- and 5- hours vs. pre). Colour represents direction (red = increased vs. pre, blue = decreased vs. pre).

Source Activity

Figure 4 shows the regions whose 'activity' demonstrated significant drug-by-time interaction, for each frequency band (top row), as well as showing main effects of drug (middle row) and session (bottom row). Significant interaction effects on activity were observed in theta (n=23), alpha (19), delta (14), beta (10) and gamma[1] (2). The spatial distribution of these effects was more widespread than in the connectivity analysis but predominantly occipital and frontal across delta, theta, alpha and beta. Regions whose activity demonstrated a main effect of drug were similarly spatially distributed (to the interaction effects) and included effects in alpha (n=31 regions), theta (24), delta (23), beta (6) and gamma (5). Effects were also observed in temporal and deep regions in the alpha band. Effects of session were observed across all frequency bands (beta n = 21, alpha = 19, delta = 19, theta = 17 and gamma = 3) and were more widespread. A list of the top-5 (significant) regions' activity for each frequency band, and each term (effect), are listed in supplementary table 3.

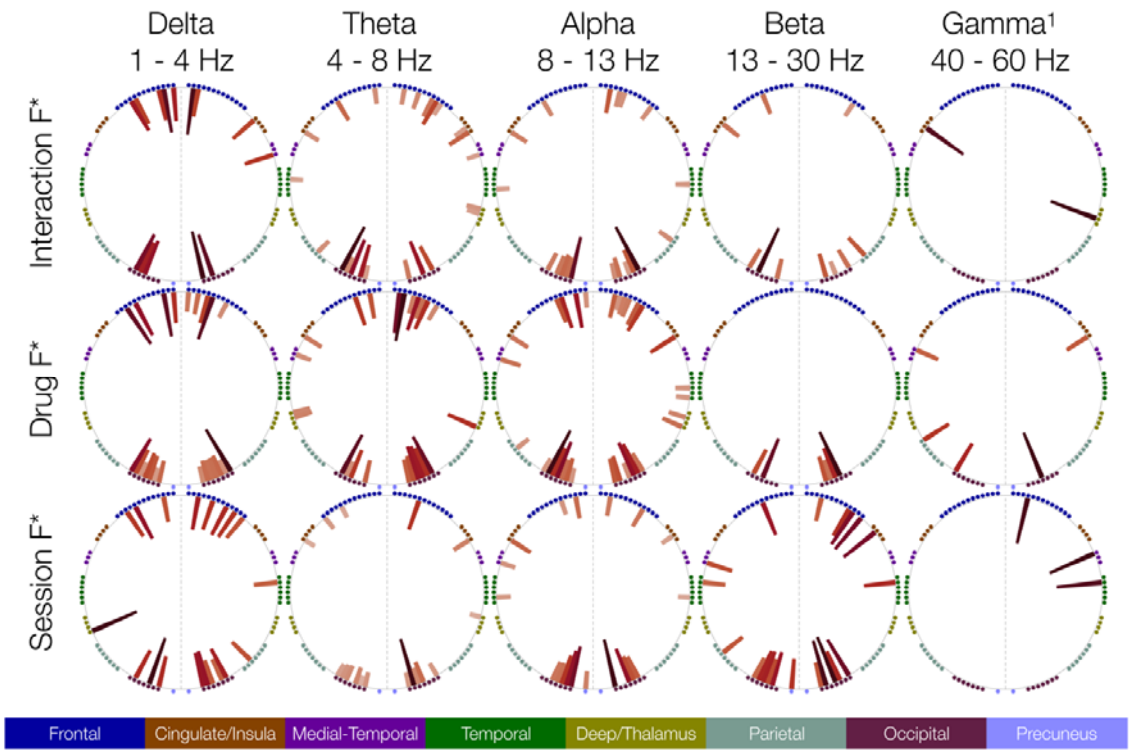

Figure 4. Topographical representation of the regions demonstrating significant (p<.05) effects on source activity (from RM-ANOVA). Showing interaction effects (top row) as well as drug (middle row) and session (bottom row) effects. Height of bars, and depth of colour, represents relative strength.

Post-hoc permutation-based randomisation testing revealed reductions of activity in posterior regions, predominantly in occipital lobe, across delta, theta (figure 5), alpha and beta (figure 6) persisting through 1-, 3- and 5-hour compared to pre, for tiagabine, but not for placebo. A list of all significant regions, for each frequency band and each comparison (n=6 comprising 1-, 3- and 5- hours vs. pre for each drug), are listed in supplementary table 4 and depicted in supplementary materials figures 1-5. For clarity, only tiagabine comparisons are shown here, in figure 5 and 6.

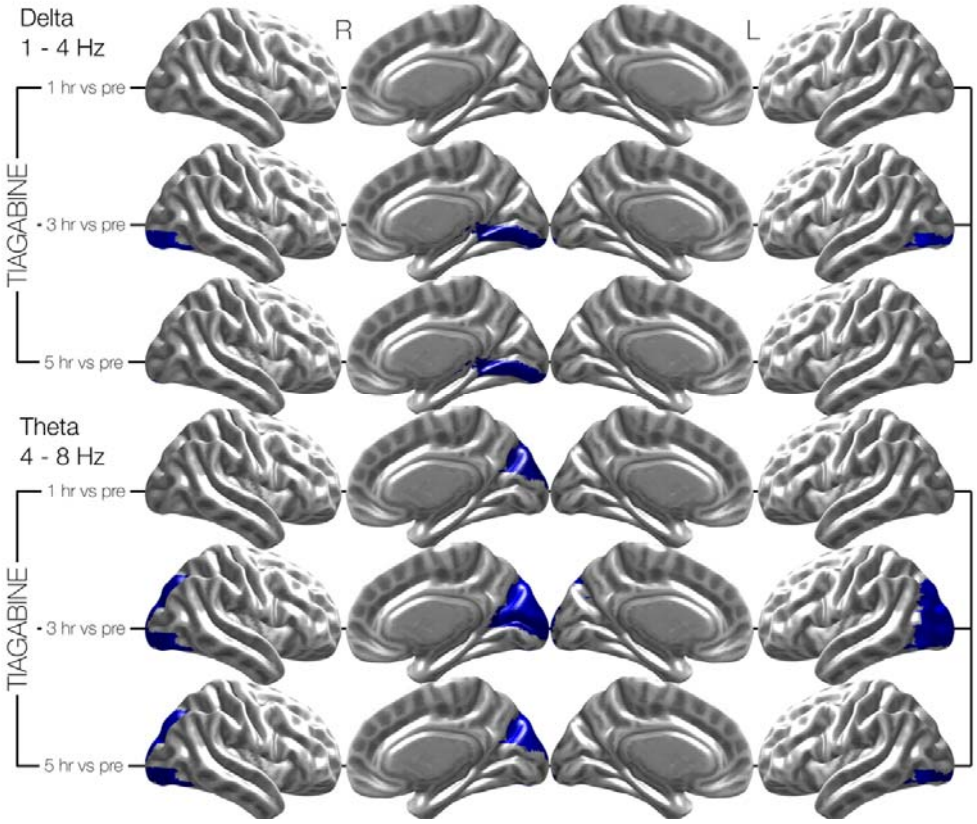

Figure 5. Parcellated brain surface rendering, demonstrating the AAL regions (parcels) of significant effect in post-hoc tests (within drug, comparing each of 1-, 3- and 5-hours post with pre) for delta and theta bands. Showing only tiagabine, because no effects were observed for placebo (see supplementary for these figures also including the placebo conditions).

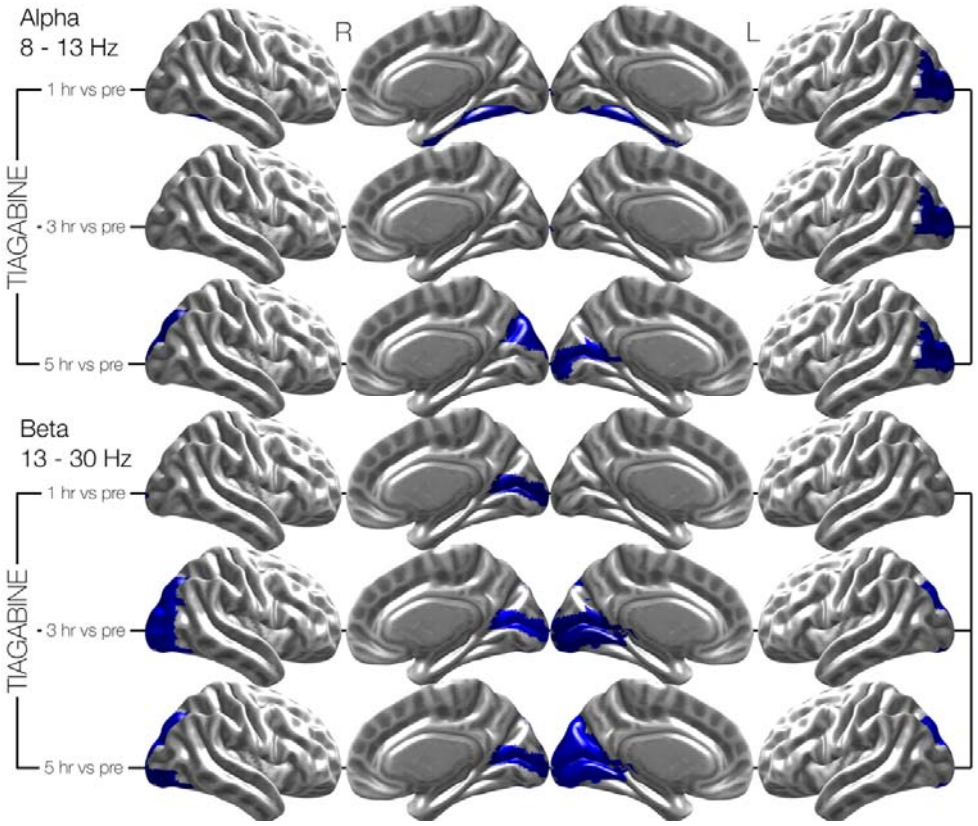

Figure 6. Parcellated brain surface rendering, demonstrating the AAL regions (parcels) of significant effect in post-hoc tests (within drug, comparing each of 1-, 3- and 5-hours post with pre) for alpha and beta bands (nothing to show for gamma). Showing only tiagabine, because no effects were observed for placebo (see supplementary for these figures also including the placebo conditions).

<u>Spatial distribution of effects and Flumazenil PET</u>

We observed significant correlations (randomisation testing with 5000 permutations and omnibus correction) in the spatial distribution of the mean drug effects on activity (i.e. absolute paired-*t* value of drug vs pre) with FMZ V_T, across delta (r=.15, 0.25 and 0.2 at 1-, 3- and 5- hours, respectively), theta (r=.15, 0.26 and 0.19 at 1-, 3- and 5- hours, respectively), alpha (r=.18, 0.22 and 0.24 at 1-, 3- and 5- hours, respectively) and beta (r=.21, 0.23 and 0.24 at 1-, 3- and 5- hours, respectively). These correlations, performed at the voxel level, suggested drug effects on activity were bigger in regions with higher FMZ V_T (figure7).

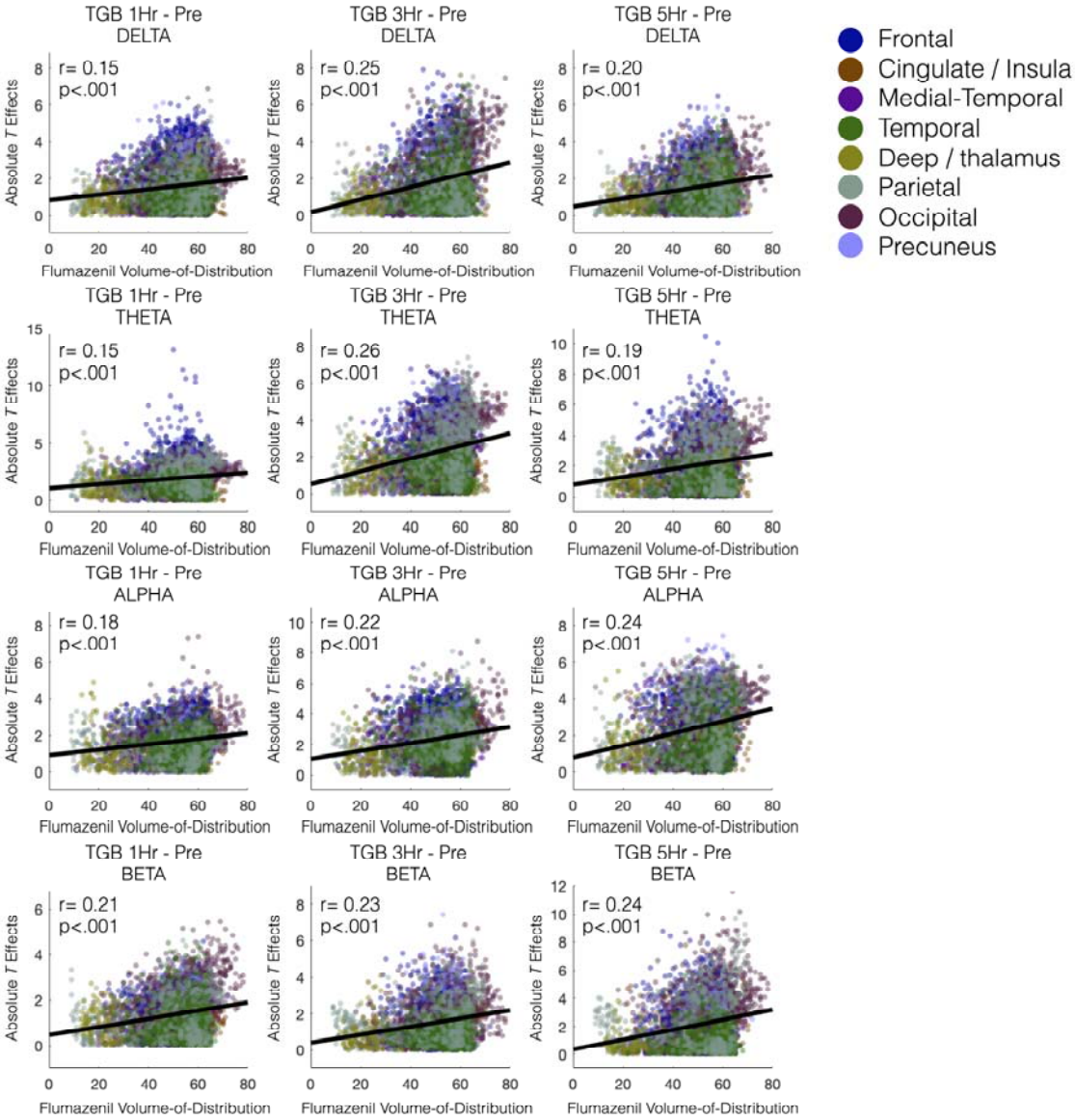

Figure 7. Voxel-wise spatial distribution of flumazenil FMZ V_T correlations with effects of drug (absolute *t* value) on activity across frequency bands delta (top), theta, alpha and beta (bottom). Dots represent individual voxels, colour coded by AAL region to which they belong. Statistics (r and p-value) are derived from randomisation-corrected Pearson correlations with omnibus correction for multiple comparisons.

Discussion

Our results indicate that pharmacologically increased GABA availability leads to reductions of both local activity and regional connectivity across low frequencies from delta, through to higher, beta frequencies. These effects are spatially co-localised to posterior brain regions, with predominant effects in occipital lobe. Figure 8 summarises the time course of mean effects for both the activity (8A) and connectivity (8B), averaged across occipital regions, showing delta, theta, alpha and beta.

As summarised in figure 8, the effects of tiagabine across the four frequency bands show similar temporal pattern, suggesting a common mechanism for the observed effects that is not highly band-limited. This wide-band effect is consistent with theories of GABAergic function as a crucial component of oscillation generation, whereby inhibitory GABAergic currents exert temporal control over principal excitatory populations.

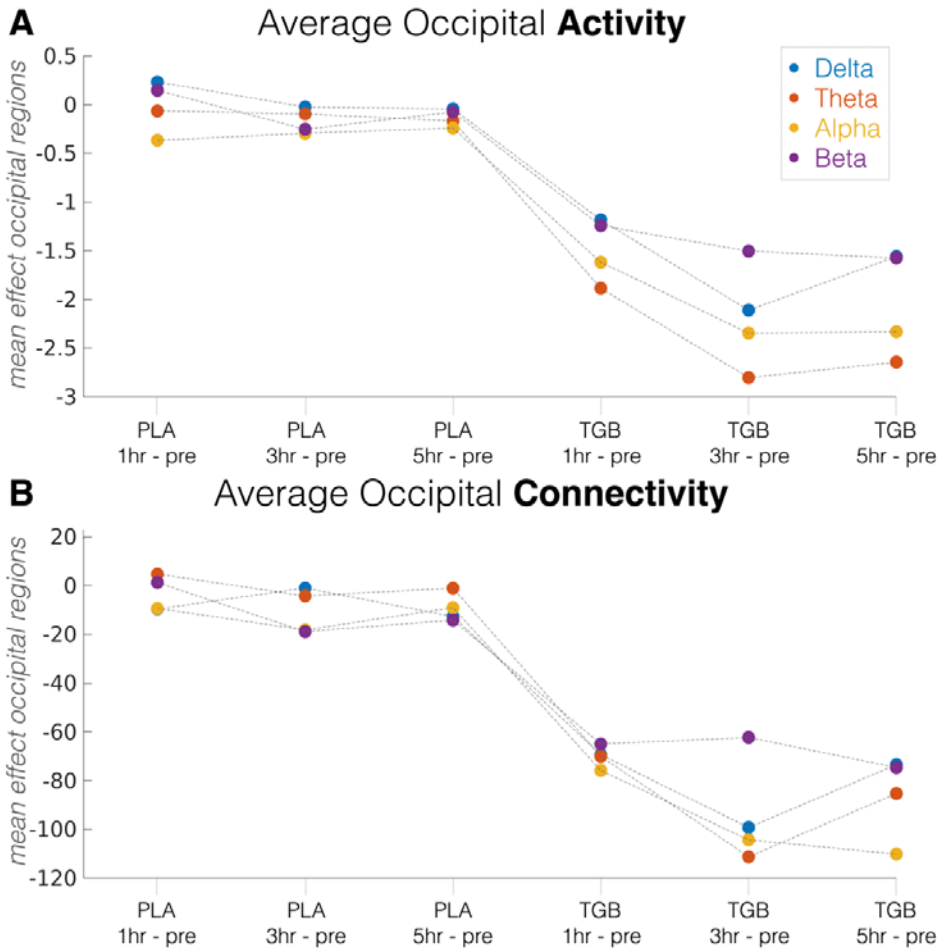

Figure 8. Time course of mean occipital effects for post-drug vs. baseline for placebo and tiagabine. Top (A) shows activity, bottom (B) shows connectivity. Averaged over occipital regions. Colours represent frequency bands.

Using a 'template' map of flumazenil V_T, which is a quantitative measure of flumazenil binding at $GABA_A$ receptors, we demonstrated that the distribution of drug-induced effects in activity, as measured by the absolute paired-*t* value of post-drug vs pre, correlated with the distribution of $GABA_A$ receptors across the brain (summarised in figure 7). In other words, regions with higher flumazenil binding also demonstrated bigger effects of drug on activity in delta, theta, alpha and beta bands. The 'time course' of this correlation across MEG session is summarised in figure 9.

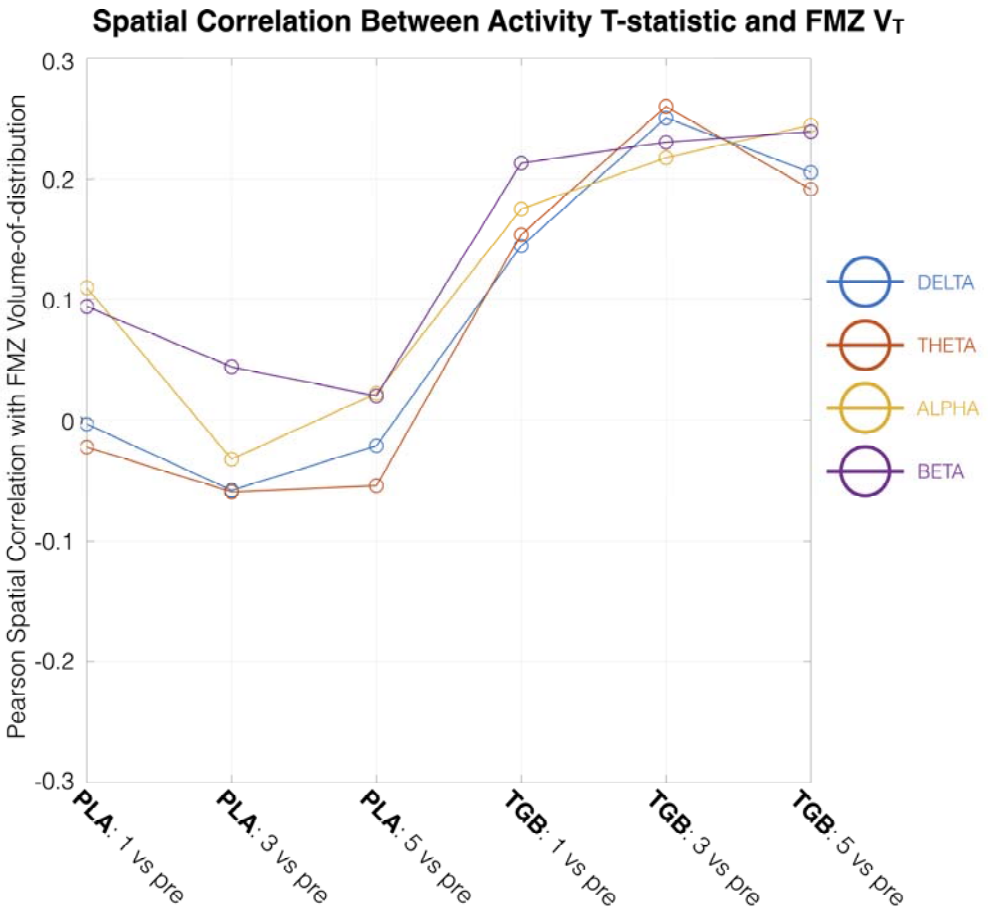

Figure 9. Summarising the spatial correlation of flumazenil volume-of-distribution with drug effects on activity across MEG sessions. Individual correlations for the tiagabine sessions are shown in figure 8.

Previous studies have suggested that tiagabine is inactive at $GABA_A$ sites, instead exerting effects on the GABAergic system through inhibiting reuptake of GABA predominantly through GABA transporter 1 (GAT1) (Madsen et al., 2011; Ransom & Richerson, 2009) and the extrasynaptic GABA transporter BGT1 (Madsen et al., 2011).

Despite this lack of binding profile at $GABA_A$ sites, tiagabine increases the decay time of $GABA_A$ mediated inhibitory postsynaptic currents (IPSCs) (Thompson & Gähwiler, 1992) and increases the affinity of $GABA_A$ receptors containing the benzodiazepine site to GABA (Frankle et al., 2009). This is important, since it links increased availability of GABA (through inhibited reuptake) to a functional effect or consequence, in the form of increased affinity and IPSC decay time. In other words, it demonstrates that merely increasing the amount of GABA with tiagabine does have a downstream effect on GABAergic function, via a $GABA_A$ mediated phenomenon. As such, our findings of tiagabine-attenuated functional connectivity and activity at low frequencies across posterior cortex may reflect enhanced GABAergic function in the form of lengthened IPSCs. The correlation in spatial effects between activity and (template, canonical) FMZ V_T supports this, because the effects are spatially colocalised to regions with a higher density of $GABA_A$ receptors.

Inclusion of template flumazenil V_T data allowed us to go a step further than quantifying changes in connectivity with enhanced GABA, because we were able to evidence that the amount of functional change in a region was predicted by that regions' canonical density of $GABA_A$ receptors. This provided a mechanistic link between the drug target and observed response, clearly demonstrating target-engagement.

Although we observed connectivity changes across frequency bands ranging from delta to beta, we observed no connectivity changes in the gamma band, even when sub-dividing into discrete 40 Hz windows. One explanation for this, is that the GABAergic processes altered by tiagabine did not disrupt the generative mechanisms of gamma oscillations. However, this is unlikely since the generation of (and spectral characteristics of) gamma oscillations are coupled to $GABA_A$ dynamics (Bartos et al., 2007; M. A. Whittington et al., 2000). Instead, we propose that gamma oscillations, which are considered locally-generated phenomena within cortical columns, are harder to measure between-region. This is because gamma oscillations, by virtue of being fast, can exist more transiently than lower frequencies, and therefore harder to detect when correlating long amplitude envelopes. If this is the case, methods aimed at identifying fast dynamical switching, such as Hidden Markov Models, may be more successful for quantifying faster frequencies (Baker et al., 2014).

Limitations

This study used a template of flumazenil V_T derived from existing data, and from different subjects to those who took part in the tiagabine MEG study. Using averaged PET data as a canonical reference map of $GABA_A$ density across the brain permitted us to compare to the average distribution of drug effects across the brain, but lacks the specificity afforded by having PET and MEG on the same individuals. Future studies should consider this, since having both would allow for detailed analysis of individual differences. A caveat here is the relative expense and exposure to radioactivity with PET compared with the safety of M/EEG.

Our correlation-based investigation of the spatial co-distribution of functional connectivity / activity with FMZ V_T, may be overestimated due to the inherent smoothness in the PET images. This smoothness-induced autocorrelation reduces the effective degrees of freedom, thereby rendering inflated statistics in conventional correlation measures, such as the Pearson's correlation employed here (Afyouni et al., 2019; Arbabshirani et al., 2014). The extent to which our result suffers this problem is unclear, since the degree to which whole brain smoothing effects the (spatial) autocorrelation of atlas-reduced data is also unclear.

Conclusions

We have demonstrated that pharmacologically increased GABA availability led to reduced activity – and inter-region connectivity – across multiple frequency bands. The spatially distinct pattern of activity changes correlated with the distribution of $GABA_A$ receptors across the brain. We propose a

mechanistic explanation for our results, whereby increased GABA availability (by tiagabine) led to increased affinity of $GABA_A$ receptors for GABA (Frankle et al., 2009), lengthening IPSCs (Thompson & Gähwiler, 1992) and consequently reducing low frequency oscillatory activity and connectivity (by the lengthened IPSCs 'dampening' current fluctuations underpinning macroscopic oscillations). While demonstrating a role for GABAergic dynamics in shaping the activity and topography of functional connectivity, we have also provided an example of MEG-based connectivity as a tool for electrophysiological receptor mapping.

Acknowledgements

ADS & HC are supported by a Wellcome Strategic Award (104943/Z/14/Z).

The brain surfaces in this paper were rendered using the SourceMesh toolbox (https://github.com/alexandershaw4/SourceMesh)

References

Afyouni, S., Smith, S. M., & Nichols, T. E. (2019). Effective degrees of freedom of the Pearson's correlation coefficient under autocorrelation. *NeuroImage*, *199*, 609–625. https://doi.org/10.1016/j.neuroimage.2019.05.011

Arbabshirani, M. R., Damaraju, E., Phlypo, R., Plis, S., Allen, E., Ma, S., Mathalon, D., Preda, A., Vaidya, J. G., Adali, T., & Calhoun, V. D. (2014). Impact of autocorrelation on functional connectivity. *NeuroImage*, *102*, 294–308. https://doi.org/10.1016/j.neuroimage.2014.07.045

Atallah, B. V., & Scanziani, M. (2009). Instantaneous Modulation of Gamma Oscillation Frequency by Balancing Excitation with Inhibition. *Neuron*, *62*(4), 566–577. https://doi.org/10.1016/j.neuron.2009.04.027

Baker, A. P., Brookes, M. J., Rezek, I. A., Smith, S. M., Behrens, T., Smith, P. J. P., & Woolrich, M. (2014). Fast transient networks in spontaneous human brain activity. *ELife*, *2014*(3), 1–18. https://doi.org/10.7554/eLife.01867

Bartos, M., Vida, I., & Jonas, P. (2007). Synaptic mechanisms of synchronized gamma oscillations in inhibitory interneuron networks. *Nature Reviews. Neuroscience*, *8*(1), 45–56.

Belelli, D., Harrison, N. L., Maguire, J., Macdonald, R. L., Walker, M. C., & Cope, D. W. (2009). Extrasynaptic GABAA Receptors: Form, Pharmacology, and Function. *Journal of Neuroscience*, *29*(41), 12757–12763.

Brunel, N., & Wang, X.-J. (2003). What determines the frequency of fast network oscillations with irregular neural discharges? I. Synaptic dynamics and excitation-inhibition balance. *Journal of Neurophysiology*, *90*(1), 415–430. https://doi.org/10.1152/jn.01095.2002

Buzsáki, G., Anastassiou, C. A., & Koch, C. (2012). The origin of extracellular fields and currents—EEG, ECoG, LFP and spikes. *Nature Reviews. Neuroscience*, *13*(6), 407–420.

Buzsáki, G., Draguhn, A., & Buzsaki, G. (2004). Neuronal oscillations in cortical networks. *Science*, *304*(5679), 1926–1929. https://doi.org/10.1126/science.1099745

Campbell, A. E., Sumner, P., Singh, K. D., & Muthukumaraswamy, S. D. (2014). *Acute Effects of Alcohol on Stimulus-Induced Gamma Oscillations in Human Primary Visual and Motor Cortices*. 1–10.

Colclough, G. L., Brookes, M. J., Smith, S. M., & Woolrich, M. W. (2015). A symmetric multivariate leakage correction for MEG connectomes. *NeuroImage*, *117*, 439–448. https://doi.org/10.1016/j.neuroimage.2015.03.071

Colclough, G. L., Woolrich, M. W., Tewarie, P. K., Brookes, M. J., Quinn, A. J., & Smith, S. M. (2016). How reliable are MEG resting-state connectivity metrics? *NeuroImage*, *138*, 284–293. https://doi.org/10.1016/j.neuroimage.2016.05.070

Cunningham, V. J., & Jones, T. (1993). Spectral analysis of dynamic PET studies. *Journal of Cerebral Blood Flow and Metabolism*, *13*(1), 15–23. https://doi.org/10.1038/jcbfm.1993.5

Frankle, W. G., Cho, R. Y., Narendran, R., Mason, N. S., Vora, S., Litschge, M., Price, J. C., Lewis, D. A., & Mathis, C. A. (2009). Tiagabine Increases [11C]flumazenil Binding in Cortical Brain Regions in Healthy Control Subjects. *Neuropsychopharmacology*, *34*(3), 624–633. https://doi.org/10.1038/npp.2008.104

Galarreta, M., & Hestrin, S. (1998). *Frequency-dependent synapt ic depression and t he balance of excit at ion and inhibit ion in t he neocort ex*. 587–594.

Halgren, M., Devinsky, O., Doyle, W. K., Bastuji, H., Rey, M., Mak-McCully, R., Chauvel, P., Ulbert, I., Fabo, D., Wittner, L., Heit, G., Eskandar, E., Mandell, A., & Cash, S. S. (2017). The Generation and Propagation of the Human Alpha Rhythm. *BioRxiv*, 202564–202564. https://doi.org/10.1101/202564

Hall, S. D., Stanford, I. M., Yamawaki, N., McAllister, C. J., Rönnqvist, K. C., Woodhall, G. L., & Furlong, P. L. (2011). The role of GABAergic modulation in motor function related neuronal

network activity. *NeuroImage*, *56*(3), 1506–1510. https://doi.org/10.1016/j.neuroimage.2011.02.025

Hammers, A., Koepp, M. J., Richardson, M. P., Hurlemann, R., Brooks, D. J., & Duncan, J. S. (2003). Grey and white matter flumazenil binding in neocortical epilepsy with normal MRI. A PET study of 44 patients. *Brain*, *126*(6), 1300–1318. https://doi.org/10.1093/brain/awg138

Hammers, A., Panagoda, P., Heckemann, R. A., Kelsch, W., Turkheimer, F. E., Brooks, D. J., Duncan, J. S., & Koepp, M. J. (2008). [11C]Flumazenil PET in temporal lobe epilepsy: Do we need an arterial input function or kinetic modeling? *Journal of Cerebral Blood Flow and Metabolism*, *28*(1), 207–216. https://doi.org/10.1038/sj.jcbfm.9600515

Kohl, M. M., & Paulsen, O. (2010). The roles of GABABreceptors in cortical network activity. *Advances in Pharmacology*. https://doi.org/10.1016/S1054-3589(10)58009-8

Kramer, M. A., Roopun, A. K., Carracedo, L. M., Traub, R. D., Whittington, M. A., & Kopell, N. J. (2008). Rhythm generation through period concatenation in rat somatosensory cortex. *PLoS Computational Biology*, *4*(9). https://doi.org/10.1371/journal.pcbi.1000169

Krupa, M., Gielen, S., & Gutkin, B. (2014). Adaptation and shunting inhibition leads to pyramidal/interneuron gamma with sparse firing of pyramidal cells. *Journal of Computational Neuroscience*. http://eutils.ncbi.nlm.nih.gov/entrez/eutils/elink.fcgi?dbfrom=pubmed&id=25005326&retmode=ref&cmd=prlinks

Kujala, J., Jung, J., Bouvard, S., Lecaignard, F., Lothe, A., Bouet, R., Ciumas, C., Ryvlin, P., & Jerbi, K. (2015). Gamma oscillations in V1 are correlated with GABAA receptor density: A multi-modal MEG and Flumazenil-PET study. *Scientific Reports*, *5*(June), 1–12. https://doi.org/10.1038/srep16347

Lassen, N. A., Bartenstein, P. A., Lammertsma, A. A., Prevett, M. C., Turton, D. R., Luthra, S. K., Osman, S., Bloomfield, P. M., Jones, T., Patsalos, P. N., O'Connell, M. T., Duncan, J. S., & Vanggaard Andersen, J. (1995). Benzodiazepine receptor quantification in vivo in humans using [11C]flumazenil and PET: Application of the steady-state principle. *Journal of Cerebral Blood Flow and Metabolism*, *15*(1), 152–165. https://doi.org/10.1038/jcbfm.1995.17

Lorincz, M. L., Kékesi, K. A., Juhász, G., Crunelli, V., & Hughes, S. W. (2009). Temporal Framing of Thalamic Relay-Mode Firing by Phasic Inhibition during the Alpha Rhythm. *Neuron*, *63*(5), 683–696. https://doi.org/10.1016/j.neuron.2009.08.012

Madsen, K. K., Ebert, B., Clausen, R. P., Krogsgaard-Larsen, P., Schousboe, A., & White, H. S. (2011). Selective GABA transporter inhibitors tiagabine and EF1502 exhibit mechanistic differences in their ability to modulate the ataxia and anticonvulsant action of the extrasynaptic GABAA receptor agonist gaboxadol. *Journal of Pharmacology and Experimental Therapeutics*, *338*(1), 214–219. https://doi.org/10.1124/jpet.111.179671

Magazzini, L., Muthukumaraswamy, S. D., Campbell, A. E., Hamandi, K., Lingford-Hughes, A., Myers, J. F. M., Nutt, D. J., Sumner, P., Wilson, S. J., & Singh, K. D. (2016). Significant reductions in human visual gamma frequency by the gaba reuptake inhibitor tiagabine revealed by robust peak frequency estimation. *Human Brain Mapping*, *3896*, 3882–3896. https://doi.org/10.1002/hbm.23283

Muthukumaraswamy, S. D., Shaw, A. D., Jackson, L. E., Hall, J., Moran, R., & Saxena, N. (2015). Evidence that Subanesthetic Doses of Ketamine Cause Sustained Disruptions of NMDA and AMPA-Mediated Frontoparietal Connectivity in Humans. *Journal of Neuroscience*, *35*(33), 11694–11706. https://doi.org/10.1523/JNEUROSCI.0903-15.2015

Muthukumaraswamy, Suresh D. (2014). The use of magnetoencephalography in the study of psychopharmacology (pharmaco-MEG). *Journal of Psychopharmacology (Oxford, England)*, *June*. https://doi.org/10.1177/0269881114536790

Muthukumaraswamy, Suresh D, Myers, J. F. M., Wilson, S. J., Nutt, D. J., Hamandi, K., Lingford-Hughes, A., & Singh, K. D. (2013). Elevating Endogenous GABA Levels with GAT-1 Blockade Modulates Evoked but Not Induced Responses in Human Visual Cortex. *Neuropsychopharmacology*, *38*(6), 1105–1112.

Nutt, D., Wilson, S., Lingford-Hughes, A., Myers, J., Papadopoulos, A., & Muthukumaraswamy, S. (2015). Differences between magnetoencephalographic (MEG) spectral profiles of drugs acting on GABA at synaptic and extrasynaptic sites: A study in healthy volunteers. *Neuropharmacology*, *88*, 155–163. https://doi.org/10.1016/j.neuropharm.2014.08.017

Oostenveld, R., Fries, P., Maris, E., & Schoffelen, J. M. (2011). FieldTrip: Open source software for advanced analysis of MEG, EEG, and invasive electrophysiological data. *Computational Intelligence and Neuroscience*, *2011*. https://doi.org/10.1155/2011/156869

Pinotsis, D. A., Schwarzkopf, D. S., Litvak, V., Rees, G., Barnes, G., & Friston, K. J. (2013). Dynamic causal modelling of lateral interactions in the visual cortex. *NeuroImage*, *66*, 563–576.

Ransom, C. B., & Richerson, G. B. (2009). Antiepileptic Drugs: GABA Transporters as Targets of Antiepileptic Drugs. *Encyclopedia of Basic Epilepsy Research*, *28*, 66–74. https://doi.org/10.1016/B978-012373961-2.00163-6

Roopun, A. K., Middleton, S. J., Cunningham, M. O., LeBeau, F. E. N., Bibbig, A., Whittington, M. A., & Traub, R. D. (2006). A beta2-frequency (20-30 Hz) oscillation in nonsynaptic networks of somatosensory cortex. *Proceedings of the National Academy of Sciences*, *103*(42), 15646–15650.

Routley, B. C., Singh, K. D., Hamandi, K., & Muthukumaraswamy, S. D. (2017). The effects of AMPA receptor blockade on resting magnetoencephalography recordings. *Journal of Psychopharmacology*, 026988111773691–026988111773691. https://doi.org/10.1177/0269881117736915

Saxena, N., Muthukumaraswamy, S. D., Diukova, A., Singh, K., Hall, J., & Wise, R. (2013). Enhanced Stimulus-Induced Gamma Activity in Humans during Propofol-Induced Sedation. *PLoS ONE*, *8*(3), e57685–e57685.

Shaw, A. D., Moran, R. J., Muthukumaraswamy, S. D., Brealy, J., Linden, D. E., Friston, K. J., & Singh, K. D. (2017). Neurophysiologically-informed markers of individual variability and pharmacological manipulation of human cortical gamma. *NeuroImage*, *161*(December 2016), 19–31. https://doi.org/10.1016/j.neuroimage.2017.08.034

Thompson, S. M., & Gähwiler, B. H. (1992). Effects of the GABA uptake inhibitor tiagabine on inhibitory synaptic potentials in rat hippocampal slice cultures. *Journal of Neurophysiology*, *67*(6), 1698–1701.

Vargas, R. (2018). The GABAergic System: An Overview of Physiology, Physiopathology and Therapeutics. *International Journal of Clinical Pharmacology & Pharmacotherapy*, *3*(2). https://doi.org/10.15344/2456-3501/2018/142

Vrba, J. (2001). Signal Processing in Magnetoencephalography. *Methods*, *25*(2), 249–271.

Wang, X.-J. (2010). Neurophysiological and Computational Principles of Cortical Rhythms in Cognition. *Physiological Reviews*, *90*(3), 1195–1268.

Whiting, P. J. (2003). GABA-A receptor subtypes in the brain: A paradigm for CNS drug discovery? *Drug Discovery Today*, *8*(10), 445–450.

Whittington, M. a, Traub, R. D., & Jefferys, J. G. (1995). Synchronized oscillations in interneuron networks driven by metabotropic glutamate receptor activation. *Nature*, *373*(6515), 612–615. https://doi.org/10.1038/373612a0

Whittington, M. A., Traub, R. D., Kopell, N., Ermentrout, B., & Buhl, E. H. (2000). Inhibition-based rhythms: Experimental and mathematical observations on network dynamics. *International Journal of Psychophysiology*, *38*(3), 315–336. https://doi.org/10.1016/S0167-8760(00)00173-2

Xing, D., Yeh, C.-I., Burns, S., & Shapley, R. M. (2012). Laminar analysis of visually evoked activity in the primary visual cortex. *Proceedings of the National Academy of Sciences*, *109*(34), 13871–13876.

Zilles, K., & Palomero-Gallagher, N. (2017). Multiple transmitter receptors in regions and layers of the human cerebral cortex. *Frontiers in Neuroanatomy*, *11*(September), 1–26. https://doi.org/10.3389/fnana.2017.00078